On statistical properties of bed load sediment concentration

Alessio Radice,[1] Francesco Ballio,[1] and Vladimir Nikora[2]

Received 30 May 2008; revised 10 March 2009; accepted 16 March 2009; published 2 June 2009.

[1] Data from a long-duration laboratory experiment involving optical measurements of moving particles in a bed load layer are presented. The data analysis is focused on identification of (1) the effects of the spatial measuring scale on concentration estimates, (2) statistical and scaling properties of sediment concentration, and (3) relationships between near-bed turbulent flow and sediment motion. The obtained results are integrated into a conceptual model that can be instrumental in studying statistical properties of solid transport rate, which, in most cases, can be linearly associated with the particle concentration.

Citation: Radice, A., F. Ballio, and V. Nikora (2009), On statistical properties of bed load sediment concentration, Water Resour. Res., 45, W06501, doi:10.1029/2008WR007192.

1. Introduction

[2] Since the pioneering works of Shields [1936], Einstein [1950], and E. Meyer-Peter and R. Müller (Formulas for bed-load transport, paper presented at Second Meeting, International Association of Hydraulic Engineering and Research, Stockholm, 1948) many empirical and phenomenological formulations for predicting solid discharge in open channels have been proposed. However, the estimates of the solid transport rate using these conventional equations proved to be highly uncertain [e.g., Gomez and Church, 1989; Martin, 2003], leading to increased attention to the small-scale details of sediment transport, which could help in advancing the existing relationships.

[3] On the basis of the Lagrangian approach, it has been found that for a given flow condition there is little dependence of the particle velocity on the particle size [e.g., Drake et al., 1988; Nikora et al., 2002; Frey et al., 2003]. In addition, using the Eulerian approach, Radice and Ballio [2008] found that the physical velocity of uniform bed load particles is only weakly dependent on the shear stress conditions at the bed, at least under low bed load transport. The highlighted behavior of the particle velocity suggests that the particle concentration should be the key factor of bed load since the sediment transport rate is proportional to the product of velocity and concentration of moving particles [e.g., Van Rijn, 1984; Niño and Garcìa, 1998; Parker et al., 2003; Ancey et al., 2008]. Indeed, given the weak dependence of the particle velocity on the flow conditions in their experiments, Ancey et al. [2008] concluded that the dynamics of the sediment transport rate may be entirely represented by that of the sediment concentration.

[4] Thus, the analysis in this Technical Note is focused on the bed particle concentration, as the most intriguing and at the same time least studied quantity involved in the sediment flux. We first present the results of an experiment with weak one-dimensional bed load, and then propose a conceptual interpretation of sediment concentration dynamics.

2. Experiments

[5] The bed load experiment used in this Technical Note has been conducted at the Hydraulic Engineering Laboratory of the Politecnico di Milano. We used a pressurized, transparent duct whose cross section is 0.40 m wide and 0.16 m deep; the duct length is almost 6 m. Approximately midway along the duct, a recess section is installed, which is filled with uniform plastic cylindrical particles of a density equal to 1.43 times that of water. Median equivalent size of the particles (i.e., diameter of a sphere of an equal volume) is d_{50} = 3.6 mm. In the remaining parts of the duct, the plastic particles were glued to the bed surface to ensure homogeneity in bed roughness.

[6] The described experimental setup differs, owing to flow pressurization, from those typically used in sediment transport research. In this respect it is useful to note that the literature on sediment transport in covered flows [e.g., Lau and Krishnappan, 1985; Smith and Ettema, 1997] indicates that sediment transport dynamics is not significantly different from that for free-surface flows. For both flow types, definitions of the threshold condition are conceptually the same. In our study, we defined the critical condition as described by Radice and Ballio [2008]; that is, we associated the incipient motion with the dimensionless solid discharge per unit width predicted by the Meyer-Peter and Müller (presented paper, 1948) equation for the Shields parameter (ratio of the Shields number to the threshold one) of 1.01. The threshold solid discharge was 6□10$^{\square 5}$, and the corresponding water discharge was 18.95 l/s.

[7] We performed a sediment transport experiment with a water discharge of 21.0 l/s. Thus, the corresponding Shields parameter can be estimated, approximately, as 1.2, assuming that for no-bed form conditions it is equal to the squared ratio of the acting flow rate to the critical flow rate. As the bed load was low, bed degradation during experimental runs was negligible and thus no sediment circulation was implemented. The sediment motion was filmed from the top to cover the bed area 20 □ 35 cm^2 (referred below as a measurement window). The instantaneous velocity profiles

[1]Dipartimento di Ingegneria Idraulica, Ambientale, Infrastrutture Viarie, Rilevamento, Politecnico di Milano, Milan, Italy.
[2]School of Engineering, University of Aberdeen, Aberdeen, UK.

0043-1397/09/2008WR007192$09.00

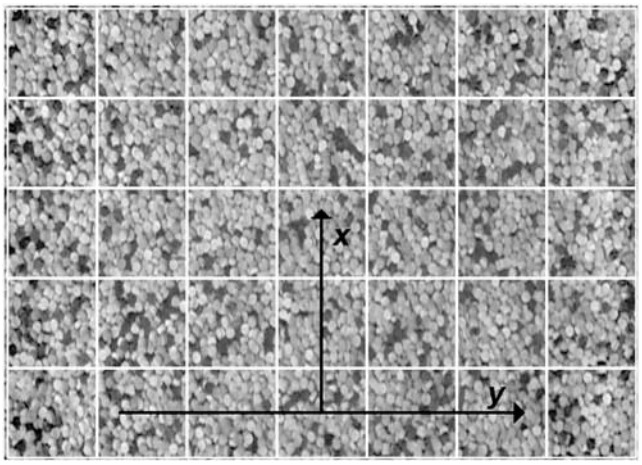

Figure 1. Sample frame of the moving grains, with (4 cm × 4 cm) measuring grid superimposed. The coordinate system used is shown. Water flow is along the x direction.

were measured at a single location using an Ultrasonic Doppler Profiler (UDP) positioned at an angle of 75° to the upper duct wall, oriented upstream. The UDP provided along-beam velocity data, that is, along the inclined coordinate aligned with the UDP. Both bed images and velocity profiles were sampled at 25 Hz frequency. The experiment duration, under constant background conditions, was 20 min, thus providing 30,000 instantaneous values of stationary data for each measured quantity. The measurement duration was chosen to secure sufficient data sets for estimating spectra and higher-order statistics. The period of prevailing velocity fluctuations (i.e., ''bursting period'') can be estimated as $T_B = k \cdot d/U_{max}$, with k ranging from 2 to 5 [Nezu and Hakagawa, 1993]. These fluctuations have been well resolved in our measurements, which were made with 0.04 s sampling intervals (25 Hz). Indeed, with U_{max} = 37 cm/s and d = h/2 = 8 cm (half the duct height), we obtain T_B = 0.4–1.1 s. However, particular turbulent events such as ejections or sweeps have been only partially resolved. According to Nikora and Goring [2000], the ratio of the event duration to the bursting period is approximately 0.07–0.09 near the bed, so that the event duration should be, in our case, around 0.03–0.08 s. Thus, the sampling frequency and duration in our measurements were appropriate to capture large-scale turbulence structures and their variability while smaller-scale short-lived events have been only partially measured. The bulk flow conditions can be characterized as steady, subcritical, fully turbulent and hydraulically rough; that is, Re = Uh/n = 52,500, $Re_p = u^* d_{50}/n \approx 100$, and $Fr = U/(gh)^{0.5} = 0.27$, where Re, Re_p, and Fr are the Reynolds, particulate Reynolds and Froude numbers, respectively, U is cross-sectional mean velocity, h is depth, n is fluid viscosity, u* is shear velocity, and g is the acceleration due to gravity.

[8] The areal concentration of moving sediments C was measured as proposed by Radice et al. [2006]. Sediment concentration is defined as a spatially averaged quantity over an averaging area A, being $C = W/(A \cdot d_{50})$, where W is the total volume of the moving particles. The number of moving grains, which is easily convertible to the corresponding solid volume, was measured by identification of the moving particles through subtraction of consecutive frames and suitable filtering of the obtained difference images. The particle diameter is used as a characteristic height of the moving layer as at low bed load intensity the particle motion occurred in a single-particle layer. Note that this selection has no effect on the statistics reported in this paper.

[9] We explored a range of averaging areas, from 1 cm^2 to 64 cm^2. An example of a studied sediment field with an averaging area of 4 × 4 cm^2 is shown in Figure 1. The double-averaged (i.e., space-time-averaged [Nikora et al., 2007]) values of the sediment concentration and particle velocity were used to check homogeneity of the sediment transport within the measurement window. The first- and second-order statistics of the sediment concentration are depicted in Figure 2, where the coefficient of variation is defined as the ratio of the standard deviation to the mean. The data show that the sediment transport is fairly uniform in the longitudinal direction, with some heterogeneity in the transverse direction (across the flow). Such heterogeneity could be expected owing to sidewall effects.

3. Scale Effects in Sediment Concentration Dynamics

[10] In this section we analyze how the statistical properties of the sediment concentration are affected by the spatial averaging area A. We first provide some general comments and then demonstrate the scale effects using our data.

[11] If we consider an area corresponding to a single grain, the probability to observe a nonzero value of concentration at a certain instant will be linked to the motion of single particles. With increasing the averaging area, the probability of a nonzero concentration at a certain instant increases, owing to increase in the number of simultaneously moving particles within the averaging area. Therefore, the larger the averaging area is, the lower number of zero values in the temporal series of concentration will be observed. In addition, the level of concentration will decrease with increase in the averaging area. It can be also shown that for homogeneous concentration fields the double-averaged value of the sediment concentration does not depend on the spatial averaging area (Appendix A). It is not the case,

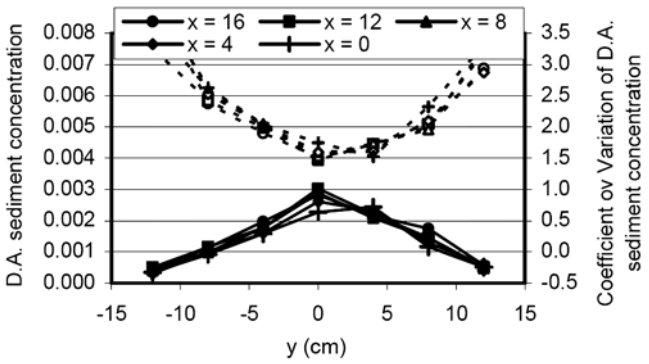

Figure 2. First- and second-order statistics of double-averaged (D.A.) sediment concentration. Mean value (solid line) and coefficient of variation (dashed line) are shown for five positions along the flow (i.e., 0, 4, 8, 12, and 16 cm).

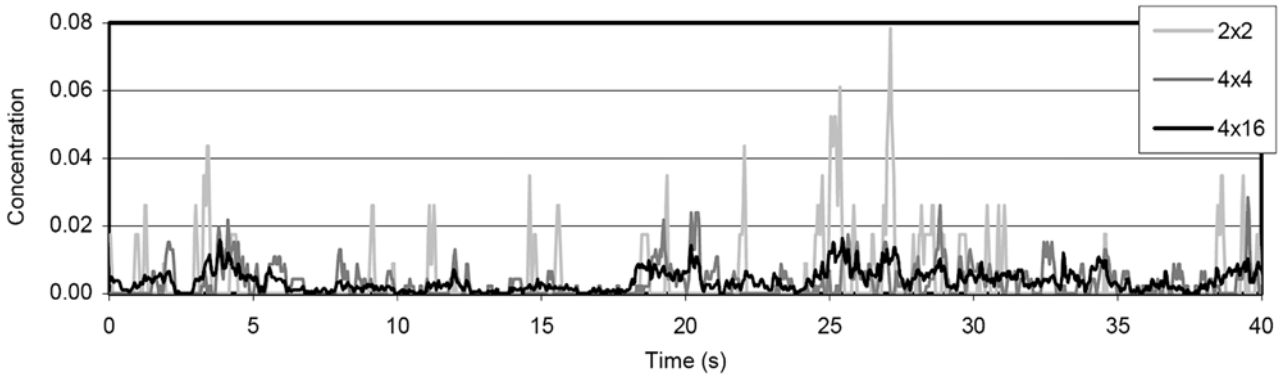

Figure 3. Temporal evolution (particular) of sediment concentration for various spatial averaging areas.

however, for the range of concentration values (expressed for example with variance) that decreases with the increasing averaging area. For spatially homogeneous noncorrelated concentration fields, the concentration variance will be proportional to the inverse averaging area (Appendix A). In a similar way, the magnitudes of the concentration spectrum and autocovariance function will be also inversely proportional to the spatial averaging area. For a more realistic scenario of spatially correlated concentration fields, this simple dependence will become more complicated owing to effects of spatial correlations.

[12] To study the scale effects on the concentration statistics the following averaging domains have been considered: 1 □ 1, 2 □ 2, 4 □ 4, 4 □ 8, 4 □ 12, and 4 □ 16 cm^2, where we reasonably assumed that effects of transverse heterogeneity were negligible within 4 cm at the channel center. Figure 3 shows examples of concentration time series for a range of the averaging areas, which illustrate considerations made above.

[13] Figure 4 demonstrates how the concentration statistics change with the spatial averaging area. As the latter increases, the double-averaged value of concentration remains approximately the same, while the variance and the coefficient of variation decrease. The trend for the variance is compared to an analytical power law with □1 exponent, with the deviation of the experimental points from the ''□1'' behavior being a predictable reflection of the spatial correlation of the concentration field (see Appendix A). Figure 5 depicts the cumulative frequency distribution of concentration values for variable spatial averaging area. It is shown that the occurrence of zero values and the maximum values measured decrease with increasing A, consistently with expectations.

[14] The autocorrelation functions of sediment concentration were found to be affected by the spatial correlations: Figure 6 presents the autocorrelation functions showing how the correlation range (i.e., correlation scale) increases with increasing averaging area. This increase of the autocorrelation length is likely to be related to the cross correlation between the concentration signals at successive longitudinal positions, reported in the following, and in turn to the persistence within the spatial averaging area of the turbulent structures responsible for the sediment motion. The spectra of the concentration time series for increasing averaging areas were also calculated and analyzed. The spectral amplitudes progressively decrease (the range of variation is more than 2 orders of magnitude) with increase in A, reflecting the decrease in the variance. In Figure 7 we present the spectra multiplied by the spatial averaging area (keeping in mind that the spectral amplitudes should be inversely proportional to the spatial averaging area if the concentration field is noncorrelated). The normalized curves are spread over 1 order of magnitude (especially at low frequencies), owing presumably to the effects of the spatial correlation of concentration. At intermediate frequencies the spectra may be fairly approximated with a power function. An increase in the averaging area extends this scaling range toward lower frequencies.

4. Statistical and Scaling Analysis of Sediment Concentration

[15] In this section we analyze the dynamics of sediment concentration with reference to the 4 □ 4 spatial averaging area. This dimension enables the small-scale characteristics to be observed without considering highly irregular temporal signals (Figure 3) as well as being comparable to the bed footprint of the UDP. We implied some conventional statistical tools together with more refined ones for detection of the scaling properties of sediment concentration. As pointed out, for example, by Singh et al. [2009], knowledge of the statistical structure of sediment transport fluctuations across scales may, among other key points, yield insight into the fundamental physics of sediment transport, support design of proper experimental campaigns, and enable comparison among different data sets. Other scholars have

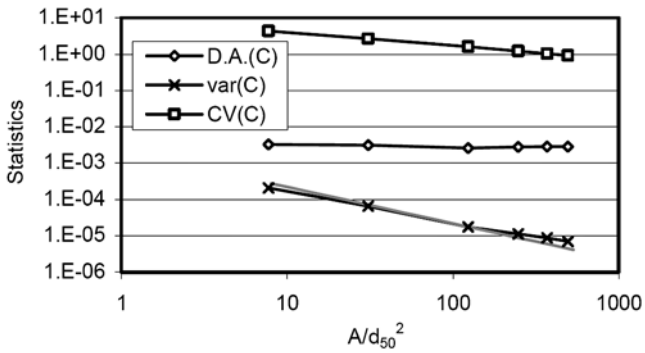

Figure 4. Statistics (double average, variance, and coefficient of variation) of sediment concentration for various spatial averaging areas. The gray line indicates a power law with -1 exponent.

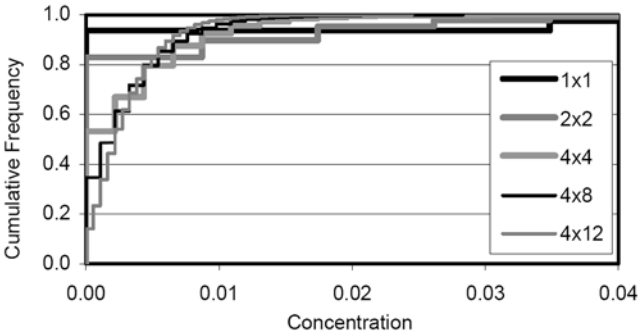

Figure 5. Cumulative frequency distributions of sediment concentration values for various spatial averaging areas.

highlighted the importance of the scaling behavior of sediment transport; for example, one can see the work of Shang and Kamae [2005] and Sivakumar [2006].

4.1. Bulk Statistics

[16] The values of the bulk statistics of the temporal series of concentration are provided for position (x = 4 cm, y = 0); the corresponding temporal signal is depicted in Figure 3 (“4 □ 4” in the legend). In our analysis we excluded the measurements related to the location (x = 0, y = 0) since the double-averaged concentration for that position was slightly lower than corresponding values for the further locations (Figure 2). The obtained bulk statistics include: double-averaged concentration of 0.0028, standard deviation of 0.0046, skewness and kurtosis coefficients of 2.53 and 12.23, respectively. The high value of the skewness coefficient is most likely due to the concentration being bounded below by the zero value and virtually unbounded above. The high value of the kurtosis coefficient reflects the variance intermittency due to infrequent extreme deviations from the mean.

4.2. Autospectra

[17] The spectrum of sediment concentration for the location centered at (x = 16 cm, y = 0) is depicted in Figure 8. We chose to plot the spectrum for this location because the latter corresponds to that of our UDP measurements, and in the following we shall compare the spectra of sediment concentration and water velocity. The spectrum of concentration can be approximated by a □5/3 power law in the frequency range from approximately 0.7 to 7 Hz, then the curve decays abruptly.

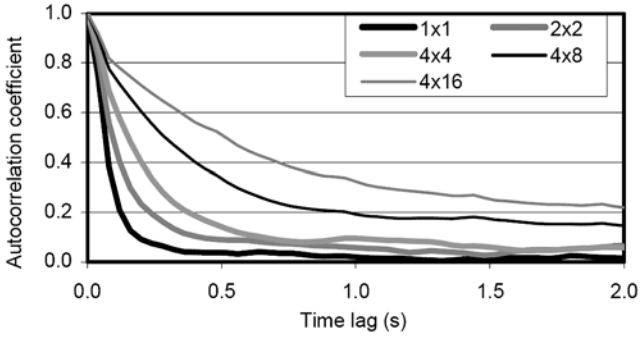

Figure 6. Autocorrelation functions of sediment concentration for various spatial averaging areas.

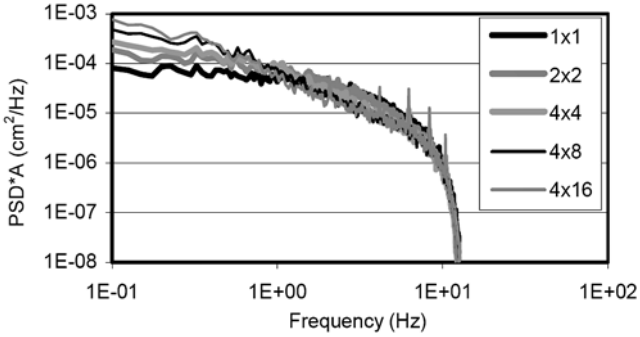

Figure 7. Spectra of sediment concentration for various spatial averaging areas. PSD indicates the power spectral density. Dimensions in the legend are in cm.

4.3. Structure Functions

[18] The time series of sediment concentration were analyzed by means of high-order generalized structure functions (GSF) [e.g., Nikora and Goring, 2001]. The pth order GSF is defined as $D_{Gp}(t) = < jDC(t)^p j >$, where t indicates the temporal lag between any two concentration values and the angular brackets indicate the average of the absolute differences in concentration values DC. When a relationship $D_{Gp}(t) / t^{pH}$ holds for a variable X, it is said that this variable exhibits a simple scaling behavior (i.e., the structure function exponent is linearly proportional to the GSF order p). In the relationship above, H is the Hurst exponent. A nonlinear relationship between the structure function exponent and the GSF order indicates a multi-scaling property of the signal [Nikora and Goring, 2001]. Benzi et al. [1993] proposed to analyze the scaling behavior of turbulent velocities by means of the Extended Self-Similarity (ESS) concept. They proposed that the existence of scaling behavior can be checked by verifying that a relationship $D_{Gp}(t) / D_{G3}(t)^{pH}$ holds. Benzi et al. [1993] showed, with reference to turbulent velocity signals, that the ESS analysis enables a clearer observation of scaling behavior compared to standard GSF plots. It was also demonstrated that the ESS approach may be useful for analysis of a range of geophysical phenomena such as channel topography or bed load fluctuations [Nikora and Goring, 2001].

[19] The GSFs were calculated for four locations (x □ 4 cm and y = 0) and then averaged (Figure 9). It was found

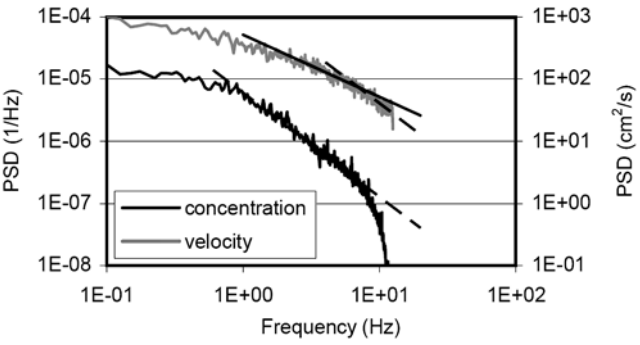

Figure 8. Spectra of sediment concentration for (x = 16 cm, y = 0) and spectra of near-bed (4 mm elevation) water velocity measured at the same (x, y) location. The dashed lines correspond to □5/3 slope, and the solid line corresponds to □1 slope.

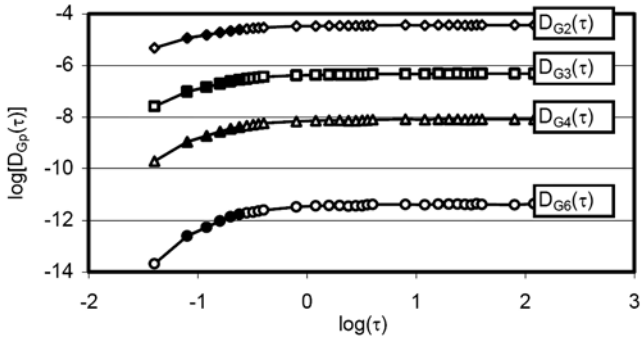

Figure 9. Generalized structure functions of the time series of sediment concentration.

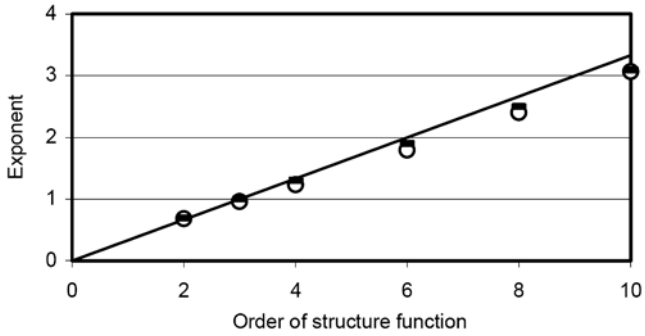

Figure 11. Scaling exponents of the time series of the sediment concentration. Open circles show the scaling range of the structure functions; black ticks show the ESS curves; and the solid line shows the Hurst exponent equal to 1/3 that is equivalent to ''□5/3'' Kolmogorov's law.

that sediment concentration shows a scaling behavior in the range 0.08 s □ t □ 0.24 s, while for larger lags the GSFs attain a saturation (scaling range indicated with black symbols in the plot). The ESS analysis is presented in Figure 10, where scaling behavior can be again recognized. Finally, in Figure 11 we show that the scaling exponents for different orders of the GSFs are quite close to the line with a 1/3 slope, showing that the Hurst exponent assumes a value of approximately 1/3. The experimental points slightly deviate from the 1/3 line for the highest-order GSFs indicating a possible multiscaling. This behavior was recognized also by Nikora and Goring [2001], even though in that case a much more evident deviation from the 1/3 line occurred for p > 5. The exponent 1/3 corresponds to Kolmogorov's ''□5/3'' law [e.g., Monin and Yaglom, 1975], in agreement with experimental spectra in Figure 8 and structure functions in Figures 9–11. Indeed, as shown by Monin and Yaglom [1975], the exponents at spectra and second-order structure functions relate to each other as g = 2H + 1 where g is a spectral exponent and 2H is the structure function exponent.

4.4. Cross-Correlation Functions

[20] A cross-correlation analysis was performed of the sediment concentration signals measured at different longitudinal locations, similar to that of Böhm et al. [2004], who studied dynamics of bed load fluctuations. Figure 12 shows the cross-correlation functions for several separation distances from the averaging area centered at (x = 4 cm, y = 0). The correlation functions exhibit a maximum which with increasing spatial separation shifts toward larger t simultaneously decreasing its magnitude. Such a behavior indicates that the concentration fluctuations propagate along the direction of sediment transport. The celerity of propagation was estimated as the ratio of the spatial separations to the time lags of maximum correlation (estimated by locally fitting parabolas to the curves). The data show that the celerity equals almost 16 cm/s, that is, more than 5 times the double-averaged sediment particle velocity (which was approximately 3 cm/s at the channel axis). The former is also higher than the time-averaged values of the near-bed longitudinal water velocity (measured via the UDP), which equals 11 cm/s at 4 mm above the bed and 13 cm/s at 6 mm above the bed.

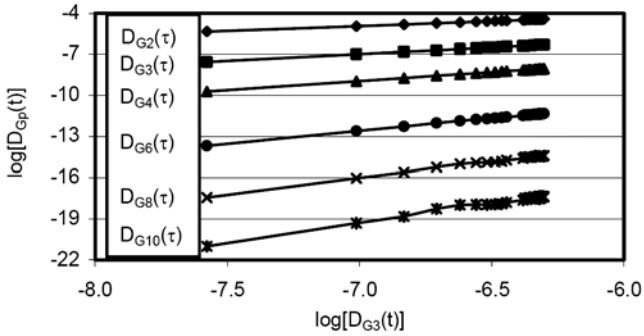

Figure 10. Extended Self-Similarity (ESS) plots of the time series of the sediment concentration.

4.5. Turbulence-Sediment Interaction

[21] The spectrum of the along-beam water velocity was calculated for an elevation of 4 mm above the granular bed (Figure 8). The spectrum can be approximated by a □5/3 power law in the range from 7 to 10 Hz, and by a □1 power law in the range from 2 to 7 Hz [e.g., Monin and Yaglom, 1975; Nikora, 1999]. A frequency range with □5/3 slope was also found for the spectrum of sediment concentration (Figure 8).

[22] The cross correlation between water velocities and sediment concentration was also investigated. This analysis, however, should be viewed as preliminary, since only the along-beam velocity values (positive when velocity is toward the probe) are available. The cross-correlation curves are shown in Figure 13 for an elevation of 4 mm above the bed (minimum available) and for an elevation approximately at half the thickness of the boundary layer

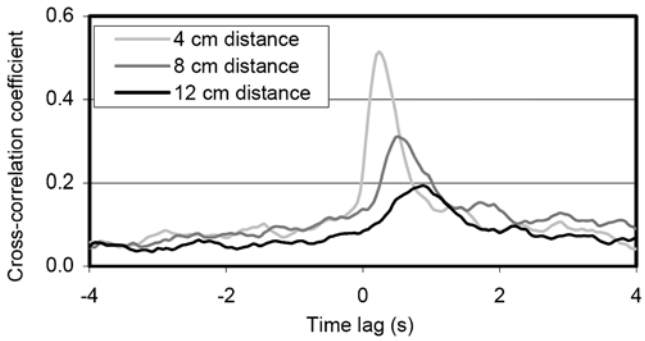

Figure 12. Cross-correlation functions of sediment concentration. Distance is in the x direction from location (x = 4 cm, y = 0).

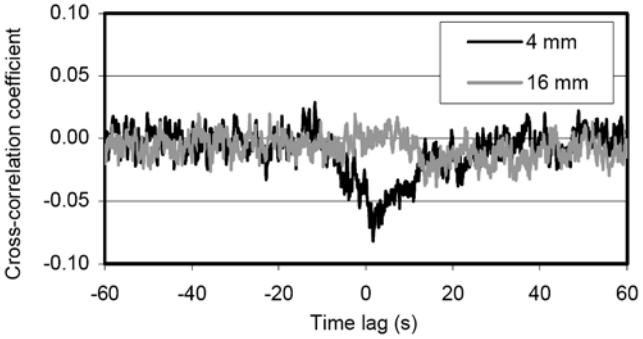

Figure 13. Cross-correlation functions between along-beam water velocity (distance from the bed indicated in the legend) and sediment concentration for (x = 16 cm, y = 0).

(the time-averaged velocity profile gives a maximum value of velocity equal to 37 cm/s for an elevation of 35 mm). The cross correlation between the velocity away from the bed and the sediment concentration is low (analogous behavior was found for elevations higher than that shown). On the contrary, the curve for the 4 mm elevation presents a negative peak; a similar behavior was found also for the elevations (not presented here) of 6 and 8 mm above the bed.

5. Conceptual Synthesis

[23] The main experimental findings of the present investigation can be summarized as follows: (1) The spectra of sediment concentration exhibit a range in which they can be approximated by a power law with □5/3 exponent. (2) The analysis of the generalized structure functions and of the ESS plots supports scaling behavior in sediment concentration fluctuations, with approximately simple scaling characterized by the Hurst exponent close to 1/3. (3) The patterns of the sediment concentration fluctuations migrate along the direction of the sediment transport at a celerity that is larger than time-averaged particle velocity and near-bed water velocity. (4) The sediment concentration dynamics is negatively correlated with the along-beam, near-bed water velocity, while it is negligibly correlated with the along-beam velocities at larger elevations.

[24] Our results are consistent with a picture of the sediment concentration dynamics reflecting a hierarchy of turbulent eddies and thus being a dynamic footprint of the turbulent flow structure. As a support to this interpretation, we notice that exponents 1/3 and □5/3 (typical of turbulent flow; see the work of Monin and Yaglom [1975]) were obtained also for the concentration fluctuations. The absence of the □1 range in the concentration spectra is not clear and needs to be investigated and explained in the follow up studies. One possible explanation is that the concentration spectra are influenced by large attached eddies which are much higher than the near-bed position where the ''□1'' range is known to act. Therefore, the signature of the ''□1'' slope in the concentration spectra may be absent even if it is present in the near-bed velocity spectra.

[25] Even though our results should be considered as preliminary owing to the paucity of the turbulent flow measurements, we still can make a qualitative comparison with the findings of Nelson et al. [1995], who made a cross-correlation analysis of solid discharge and LDV measurements of the near-bed components (horizontal and vertical) of water velocity. They found a high positive correlation between the longitudinal velocity component and the solid discharge, and a low negative correlation between the vertical component and the sediment flux. They interpreted the correlations obtained assuming that the sediment flux increases when the longitudinal velocity fluctuation is positive and the vertical velocity component is downward. The latter consideration, supported by quadrant analysis, allowed them to attribute most of the sediment transport to sweep events in the boundary layer. The major role played by bursting events in sediment pickup has been also highlighted by Niño and Garcìa [1996], Sechet and Le Guennec [1999], Hurther and Lemmin [2003], among others. Our UDP probe is almost vertical (as said, it is placed at an angle of 75□), and as a result the velocity readings are largely dominated by the vertical velocity. Hence, the cross-correlation curves are similar to those found by Nelson et al. [1995] for the vertical velocity component. On the basis of this result, we may also infer that in our case the sweep-like events in the boundary layer were the major triggering factors for the sediment transport.

[26] Whatever the triggering events are, the celerity of propagation of the sediment concentration patterns is likely to be linked to the propagation of these events along the flow. The celerity of propagation is larger than the typical velocities for particles and water. As a result, when any sediment particle is put in motion at a certain location, the impulse of concentration migrates downstream faster than the grain displaced. This observation is in agreement with earlier ones presented by Drake et al. [1988], who, analyzing the bed load in a natural creek, attributed most of the sediment transport to ''sweep transport events'' whose trace on the bed was observed to travel with much bigger speed than the average water velocity.

[27] A footprint of a typical sweep event in our experiment can be estimated using the event duration (□0.05 s) and the celerity of propagation of concentration (16 cm/s), giving a representative size of 0.8 cm, which corresponds to a ratio $A/d_{50}^2 = 4.9$. Therefore, for $A/d_{50}^2 < 5$ one may expect effects of spatial correlation on concentration variance to be stronger than those seen in Figure 4; unfortunately, the relatively large size of our sediment particles prevented us from exploring smaller values of A/d_{50}^2. Figure 4 shows that there is some deviation of the variance-scale dependence from the ''□1'' law even for the averaging scales larger than $A/d_{50}^2 = 5$, which reflects large-scale correlation. Similar long-range correlations between the near-bed velocity and bed load concentration are also seen in Figure 13. These long-range correlations most probably reflect effects of large-scale turbulent structures or packets of smaller-scale events such as sweeps.

6. Conclusions

[28] The present Note documents the results of an experimental investigation of bed load sediment concentration. The analysis of the concentration was chosen as earlier studies suggest that the sediment flux dynamics be mostly dependent on the concentration of particles in motion. The sediment concentration was defined as a spatially averaged quantity, and the effect of the spatial averaging area on the resulting statistics was investigated. It was found that the spatial behavior of sediment concentration is in approximate

agreement with that expected for a homogeneously distributed, noncorrelated quantity; yet some deviations were detected, that were attributed to the spatial correlation of the sediment concentration field.

[29] With reference to the preferred size of the spatial averaging area, analysis of the statistic and scaling properties of sediment concentration was conducted and identified a number of properties not reported before. It was found that the sediment concentration exhibits a scaling behavior, characterized by exponents identical to those proposed for turbulent flow fields. Furthermore, cross-correlation analysis enabled a celerity of propagation of concentration patterns to be evaluated. This celerity was much larger than the double-averaged particle velocity and near-bed flow velocity. Finally, an analysis of the cross correlation between along-beam water velocities and sediment concentration was conducted, which revealed a negative correlation for the near-bed velocities and almost no correlation for those away from the bed.

[30] The experimental results suggest that (1) the dynamics of sediment concentration be a reflection of the turbulent eddy cascade and (2) the solid discharge be the result of the composition of displacements of different sediment particles, triggered by near-bed turbulent events.

Appendix A

[31] Let us consider concentration values at different locations defined for spatial averaging areas of the same size a; the instantaneous concentration values for these locations will be denoted as C_{ai}. We assume that the concentration field is homogeneous; that is, the temporal concentration statistics are the same for all locations considered. For a larger area A(= ma) the concentration is defined as C_A. The instantaneous concentration values at these two scales (a and A) are related as

$$C_A = \frac{1}{m}\sum_{i=1}^{m} C_{ai}, \qquad (A1)$$

showing that the instantaneous concentration at the A scale is the average of the instantaneous concentration values at the a scale. A relationship between the double-averaged concentration values follows from equation (A1):

$$\overline{C_A} = \overline{\frac{1}{m}\sum_{i=1}^{m} C_{ai}} = \frac{1}{m}\sum_{i=1}^{m} \overline{C_{ai}} = \overline{C_{ai}} = \overline{C_a}, \qquad (A2)$$

where an overbar indicates the time averaging. A relationship between the variances is derived as

$$\begin{aligned} s_A^2 &= \overline{\left(C_A - \overline{C_A}\right)^2} = \overline{\left(\frac{1}{m}\sum_{i=1}^{m} C_{ai} - \overline{C_{ai}}\right)^2} \\ &= \overline{\left(\frac{1}{m}\sum_{i=1}^{m} C_{ai} - \overline{C_{ai}}\right)^2} = \frac{1}{m^2}\sum_{i=1}^{m} \overline{\left(C_{ai} - \overline{C_{ai}}\right)^2} \\ &\quad + \frac{2}{m^2}\sum_{k=1}^{m}\sum_{n=k+1}^{m} \overline{\left(C_{ak} - \overline{C_{ak}}\right)\left(C_{an} - \overline{C_{an}}\right)} \\ &= \frac{1}{m} s_a^2 + \frac{2}{m^2}\sum_{k=1}^{m}\sum_{n=k+1}^{m} \overline{\left(C_{ak} - \overline{C_{ak}}\right)\left(C_{an} - \overline{C_{an}}\right)}; \end{aligned} \qquad (A3)$$

As can be seen in equation (A3), the variance at the A scale is the sum of two terms: (1) the product of the variance at the a scale times the ratio m between the areas A and a and (2) a term accounting for the spatial correlation of the concentration field. Thus, for a noncorrelated field we have $s_A^2 = (a s_a^2) A^{-1}$.

[32] For a correlated field, the ratio of the variance at the A scale to that at the a scale is

$$\frac{s_A^2}{s_a^2} = \frac{a}{A} + 2 s_a^2 \frac{a^2}{A^2}\sum_{k=1}^{m}\sum_{n=k+1}^{m} \overline{\left(C_{ak} - \overline{C_{ak}}\right)\left(C_{an} - \overline{C_{an}}\right)}; \qquad (A4)$$

The first term on the right-hand side is <1 and is responsible for the previously described dependence; if we reasonably assume that the second term is positive, the variance reduction will be smaller than it is in the case of noncorrelated concentration.

References

Ancey, C., A. C. Davison, T. Böhm, M. Jodeau, and P. Frey (2008), Entrainment and motion of coarse particles in a shallow water stream down a steep slope, J. Fluid Mech., 595, 83–114, doi:10.1017/S0022112007008774.

Benzi, R., S. Ciliberto, R. Tripiccione, C. Baudet, F. Massaioli, and S. Succi (1993), Extended self-similarity in turbulent flows, Phys. Rev. E, 48, R29–R32, doi:10.1103/PhysRevE.48.R29.

Böhm, T., C. Ancey, P. Frey, J. L. Reboud, and C. Ducottet (2004), Fluctuations of the solid discharge of gravity-driven particle flows in a turbulent stream, Phys. Rev. E, 69, 061307, doi:10.1103/PhysRevE.69.061307.

Drake, T. G., R. L. Shreve, W. E. Dietrich, P. J. Whiting, and L. B. Leopold (1988), Bedload transport of fine gravel observed by motion-picture photography, J. Fluid Mech., 192, 193–217, doi:10.1017/S0022112088001831.

Einstein, H. A. (1950), The bed-load function for sediment transportation in open channel flows, Tech. Bull. 1026, U. S. Dep. of Agric., Washington, D. C.

Frey, P., C. Ducottet, and J. Jay (2003), Fluctuations of bed load solid discharge and grain size distribution on steep slopes with image analysis, Exp. Fluids, 35, 589–597, doi:10.1007/s00348-003-0707-9.

Gomez, B., and M. Church (1989), An assessment of bed load sediment transport formulae for gravel bed rivers, Water Resour. Res., 25, 1161–1186, doi:10.1029/WR025i006p01161.

Hurther, D., and U. Lemmin (2003), Turbulent particle flux and momentum flux statistics in suspension flow, Water Resour. Res., 39(5), 1139, doi:10.1029/2001WR001113.

Lau, L. L., and B. G. Krishnappan (1985), Sediment transport under ice cover, J. Hydraul. Eng., 111, 934–950, doi:10.1061/(ASCE)0733-9429(1985)111:6(934).

Martin, Y. (2003), Evaluation of bed load transport formulae using field evidence from the Vedder River, British Columbia, Geomorphology, 53, 75–95, doi:10.1016/S0169-555X(02)00348-3.

Monin, A. S., and A. M. Yaglom (1975), Statistical Fluid Mechanics: Mechanics of Turbulence, MIT Press, Cambridge, Mass.

Nelson, J. M., R. L. Shreve, S. R. McLean, and T. G. Drake (1995), Role of near-bed turbulence in bed load transport and bed form mechanics, Water Resour. Res., 31, 2071–2086, doi:10.1029/95WR00976.

Nezu, I., and H. Hakagawa (1993), Turbulence in Open-Channel Flows, A. A. Balkema, Rotterdam, Netherlands.

Nikora, V. (1999), Origin of the "−1" spectral law in wall-bounded turbulence, Phys. Rev. Lett., 83, 734–736, doi:10.1103/PhysRevLett.83.734.

Nikora, V., and D. Goring (2000), Flow turbulence over fixed and weakly mobile gravel beds, J. Hydraul. Eng., 126, 679–690, doi:10.1061/(ASCE)0733-9429(2000)126:9(679).

Nikora, V., and D. Goring (2001), Extended self-similarity in geophysical and geological applications, Math. Geol., 33, 251–271, doi:10.1023/A:1007630021716.

Nikora, V., H. Habersack, T. Huber, and I. McEwan (2002), On bed particle diffusion in gravel bed flows under weak bed load transport, Water Resour. Res., 38(6), 1081, doi:10.1029/2001WR000513.

Nikora, V., I. McEwan, S. McLean, S. Coleman, D. Pokrajac, and R. Walters (2007), Double-averaging concept for rough-bed open-channel and overland flows: Theoretical background, J. Hydraul. Eng., 133, 873–883, doi:10.1061/(ASCE)0733-9429(2007)133:8(873).

Niño, Y., and M. Garcìa (1996), Experiments on particle-turbulence interactions in the near-wall region of an open channel flow: Implications for sediment transport, J. Fluid Mech., 326, 285–319, doi:10.1017/S0022112096008324.

Niño, Y., and M. Garcìa (1998), Using Lagrangian particle saltation observations for bedload sediment transport modelling, Hydrol. Processes, 12, 1197–1218, doi:10.1002/(SICI)1099-1085(19980630)12:8<1197::AID-HYP612>3.0.CO;2-U.

Parker, G., G. Seminara, and L. Solari (2003), Bed load at low Shields stress on arbitrarily sloping beds: Alternative entrainment formulation, Water Resour. Res., 39(7), 1183, doi:10.1029/2001WR001253.

Radice, A., and F. Ballio (2008), Double-average characteristics of sediment motion in one-dimensional bed load, Acta Geophys., 56, 654–668, doi:10.2478/s11600-008-0015-0.

Radice, A., S. Malavasi, and F. Ballio (2006), Solid transport measurements through image processing, Exp. Fluids, 41, 721–734, doi:10.1007/s00348-006-0195-9.

Sechet, P., and B. Le Guennec (1999), Bursting phenomenon and incipient motion of solid particles in bed-load transport, J. Hydraul. Res., 37, 683–696.

Shang, P., and S. Kamae (2005), Fractal nature of time series in the sediment transport phenomenon, Chaos Solitons Fractals, 26, 997–1007, doi:10.1016/j.chaos.2005.01.051.

Shields, A. (1936), Anwendung der Aehnlichkeitsmechanik und der Turbulenz Forschung auf die Geschiebebewegung, in Mitteilungen der Preussische Versuchanstalt für Wasserbau und Schiffbau, Rep. 26, Tech. Hochsch., Berlin.

Singh, A., K. Fienberg, D. J. Jerolmack, J. Marr, and E. Foufoula-Georgiou (2009), Experimental evidence for statistical scaling and intermittency in sediment transport rates, J. Geophys. Res., 114, F01025, doi:10.1029/2007JF000963.

Sivakumar, B. (2006), Suspended sediment load estimation and the problem of inadequate data sampling: A fractal view, Earth Surf. Processes Landforms, 31, 414–427, doi:10.1002/esp.1273.

Smith, B. T., and R. Ettema (1997), Flow resistance in ice-covered alluvial channels, J. Hydraul. Eng., 123, 592–599, doi:10.1061/(ASCE)0733-9429(1997)123:7(592).

Van Rijn, L. C. (1984), Sediment transport: Part I. Bed load transport, J. Hydraul. Eng., 110, 1431–1456, doi:10.1061/(ASCE)0733-9429(1984)110:10(1431).

F. Ballio and A. Radice, Dipartimento di Ingegneria Idraulica, Ambientale, Infrastrutture Viarie, Rilevamento, Politecnico di Milano, Piazza L. da Vinci 32, I-20133 Milan, Italy. (alessio.radice@polimi.it)

V. Nikora, School of Engineering, University of Aberdeen, AB24 3UE Aberdeen, UK.